Arabian Journal of Geosciences (2022) 15: 179
https://doi.org/10.1007/s12517-021-09281-8

ORIGINAL PAPER

Feasibility study of safe mining of thick coal seam under thick loose sediment and thin bedrock

Xianhui Wang[1,2] · **Shuyun Zhu**[1,2]

Received: 28 September 2021 / Accepted: 11 December 2021 / Published online: 17 January 2022

Abstract
In the area studied, the roof of coal seam is the combination of thick loose bed and thin bedrock, based on the analysis of strata structure and on aquifer water features, by way of analyzing the construction of rock fracture mechanics model of the overburden rock caving mechanism. On this basis, a calculation method is developed based on a mechanical model of breakage of each rock layer above the coal seam by analyzing the rock layer as a fixed beam in continuum analysis. By constructing a mechanical model with fragmented rock, the process of overburden failure and the heights of the water-conducting fracture zone and caved zones are determined. Through theoretical analysis, empirical formula and numerical simulation, the height of caved zone, and water-conducting fracture zone height in the area studied are calculated, the thickness of protective layer is determined by analogy, and finally the minimum recommended value of safe coal pillar is put forward. The research results have important practical significance for guiding coal mine safety production.

Keywords Thick loose sediment · Thin bedrock · Overburden failure · Caved zone · Water-conducting fracture zone

Introduction

With rapid advancements in mining technology in recent decades, most mines are facing the problem of rapid mining and depletion of natural resources. The Yanzhou coalfield in the Shandong Province of China which is covered by a very thick loose layer of sediment is a good example. In order to ensure the sustainable development of the mine, two mining approaches have been primarily used: deep mining and shallow mining (Ye et al. 2018; Wu et al. 2019, 2020; Huang et al. 2021). The heights of the caved and water-conducting fracture zones that formed after the deformation and failure of the overlying strata due to shallow mining have had a substantial influence on the safety and productivity of the mine (Zhu et al. 2014; Sui et al. 2015; Yang et al. 2011; Li et al. 2015).

Previous research on caved and water-conducting fracture zones can be broadly categorized as theoretical analyses (Wang et al. 2019; Zhou et al. 2019; Ju et al. 2017; Xu et al. 2021), empirical approaches (Liu et al. 2018; Zhao et al. 2018; Zeng et al. 2020; Wu et al. 2020), and numerical simulation (Sun et al. 2018; Zhao et al. 2016; Ghasemi and Shahriar, 2012; Wang et al. 2017). In terms of theoretical analyses, various hypotheses have been proposed since the end of the twentieth century to describe the impacts of the rock mass structure on the overlying strata of the stope, such as roof pressure arching theory, the suspension theory, preformed fractures, and the detached block theory (Wang et al. 2019). The voussoir beam theory was first used in a mechanical model in Chinese studies by Qian et al. (1994) prior to the use of the detached block theory (determining weight of a detached block of roof rock that is found above the entry of the mine) and the pseudo plastic beam theory on the stability of the rock strata by Cao et al. (1998) studied the effects of the position of the key strata on the height of the water-conducting fracture zone. They proposed a method to calculate the height of the water-conducting fracture zone with different mined heights, as well as the height

Responsible Editor: Zeynal Abiddin Erguler

✉ Shuyun Zhu
shyzhuqiao@163.com

[1] Key Laboratory of Coalbed Methane Resources and Reservoir Formation Process of the Ministry of Education, China University of Mining and Technology, Xuzhou, Jiangsu Province 221116, People's Republic of China

[2] School of Resources and Geosciences, China University of Mining and Technology, Xuzhou, Jiangsu Province 221116, People's Republic of China

of the water-conducting fracture zone based on structural changes of the main stratum. Guo et al. (2019) proposed a new theoretical prediction method to determine the height of the water-conducting fracture zone with block caving by constructing mechanical models to examine the process on overburden failure.

With the development of computer technology, the relevance and use of numerical simulation have increased in importance in mining studies. Many Chinese and international mining academics have used numerical simulation to predict and calculate the heights of the water-conducting fractured and caved zones and mining subsidence (Yu et al. 2020; Wu et al. 2021; Yu et al. 2019; Huang et al. 2021; Wu et al. 2021). In fact, the Yanzhou coalfield has been extensively studied and a number of numerical simulations have been carried out in the area. In this paper, we further extend current studies by theoretically calculating the heights of the water flow fractured and caved zones in the area studied. And numerical simulation is carried out, followed by a comparison of the results of the theoretical calculations, empirical calculations, and numerical simulation analysis. Numerical simulation is used to provide insights and can be used to address realistic problems with complex conditions. It is used to investigate conditions that cannot be experimentally examined in the field. Numerical simulation can also perform stress and displacement analyses. However, the boundary conditions and material properties are often simplified for analysis, which affects the results and the reason that theoretical calculations and empirical equations are used for a comparison with the numerical simulation. The feasibility of further safely mining the coal seam with coal and rock pillars for controlling sand inrush is explored because the increase in mining activities has changed the hydrogeological conditions of the aquifers in the Yanzhou mining area. We find a water poor aquifer so while prevention of water seepage is important, the coal pillars should also prevent sand flow aside from water seepage in order to increase the safety of mining.

Overview of the area studied

Location of the area studied

The southern boundary of this area studied is the working face open-off cut with a length of 282 m; the northern boundary is the stopping line with a length of 157 m; the western boundary is No. 1 exploration roadway with a length of 2505 m, and the eastern boundary is No. 2 exploration roadway with a length of 1979 m, the area of area studied is 6.0E5 m^2 (Fig. 1). The main coal seam mined in the working face is the coal seam of Permian Taiyuan, which is called No.3 coal seam. According to the drilling data in and near

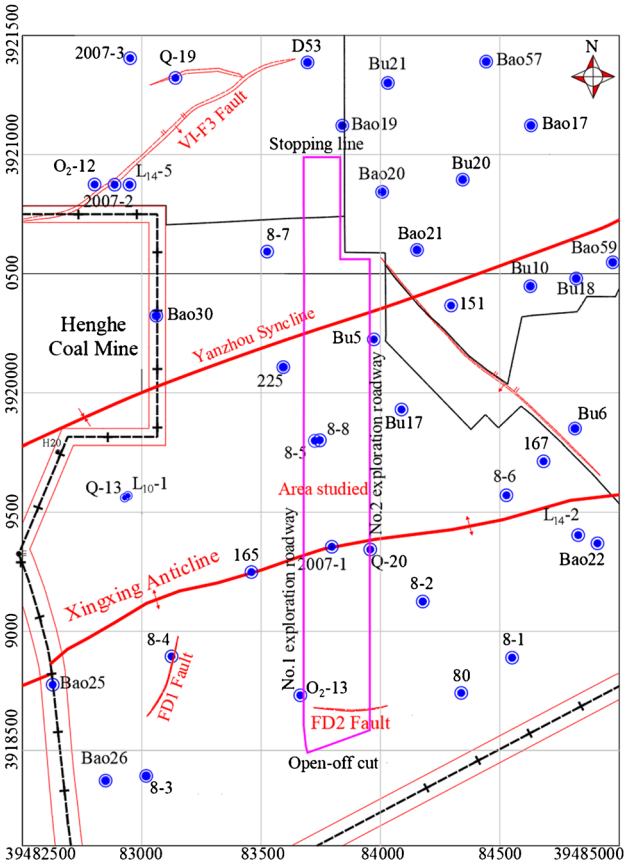

Fig. 1 Location of the area studied and distribution map of detection boreholes

the area studied, it is found that the thickness of No. 3 coal seam is 3.69 ~ 7.76 m, the average thickness of No. 3 coal seam is 5 m, and the stratigraphic dip is 7°. There are two large folding structure in the area studied, namely Xingxing Anticline and Yanzhou Syncline, and they span the area studied in an east–west direction.

Characteristics of overlying strata

The lithology of the overlying strata is shown in Fig. 2, based on the data from the borehole on the surface above the area studied. The overlying strata of No.3 coal seam is mainly divided into Quaternary system, Jurassic and Permian bedrock, and it presents a thick quaternary loose layer and a thin bedrock layer.

Characteristics of the quaternary loose layer

The thickness distribution of the quaternary loose layer is relatively stable, with an average thickness of 164.07 m. The lower tens of meters of quaternary loose layer is called

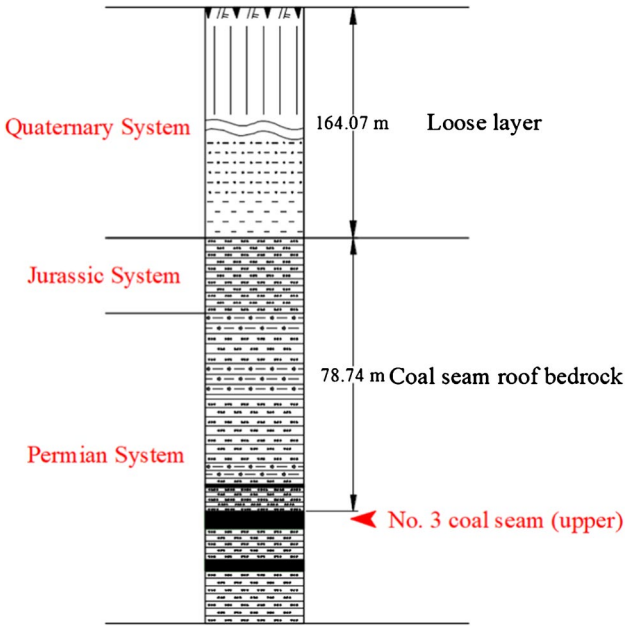

Fig. 2 Schematic diagram of coal seam roof overburden

quaternary bottom (QB). Table 1 shows the borehole detection data of QB lithology combination.

It can be seen that the thickness of sand is small, accounting for only 39.7% of the thickness of QB, and the thickness of clay is larger, accounting for 60.3% of the thickness of QB. In QB, there is usually an aquifer called quaternary bottom aquifer; the thickness distribution of the two exploration roadway is shown in Fig. 3.

The aquifer in the direction from open-off cut to stopping line showed a change characteristic of decreasing first and then increasing and finally decreasing, with an average thickness of 9.5 m. The maximum specific yield of the aquifer is 0.03 L/(s·m) by pumping test. Beneath the aquifer, there is a clay aquifuge called quaternary bottom aquifuge, and the thickness distribution of the area studied two exploration roadway is shown in Fig. 4.

There is a partial absence of this aquifuge in the northern part of the area studied. From south to north, there is a trend of increasing first and then decreasing to disappear. This aquifuge is clay with good low compressibility, plasticity, and expansibility, which can maintain good overall performance under the influence of mining, and has good ability of water and sand resistance.

Characteristics of Jurassic and Permian bedrock

The thickness of bedrock varies greatly within the study area, the thickness of bedrock decreases firstly and then increases in the direction from open-off cut to stopping line, with a minimum of 29.2 m and a maximum of 169.3 m. The bedrock is mainly composed of feldspar sandstone, quartz sandstone, and mudstone, as shown in Table 2. As can be seen from Table 2, sandstone occupies a relatively large proportion in bedrock, with an average proportion of 67.4%, while mudstone occupies a relatively small proportion of 32.6% (Fig. 5).

Table 1 Lithologic assemblage of the quaternary bottom

Borehole	*QB* thickness (m)	Sand thickness (m)	Percentage of sand thickness (%)	Clay thickness (m)	Percentage of clay thickness (%)
O_2-13	42.6	9.6	33.0	22.5	77.5
165	27.5	10.8	16.7	39.3	60.7
2007–1	40.7	9.9	30.8	24.3	75.7
8–5	42.2	15.3	26.9	36.3	63.7
225	18.8	8.1	10.7	43.1	56.9
8–7	41.3	22.8	18.5	55.2	44.8
8–1	40.7	23.1	17.6	56.7	43.3
8–2	42.9	16.5	26.4	38.4	61.6
8–3	41.4	17.2	24.2	41.5	58.5
8–4	43.2	13.4	29.8	31.1	68.9
8–6	39.7	17.0	22.7	42.8	57.2
L_{14}-1	24.3	8.9	15.4	36.6	63.4
Bao30	39.7	25.7	14.0	64.7	35.3
Q-13	27.4	11.0	26.4	29.4	70.6
Q-20	41.3	13.6	27.7	32.9	67.1

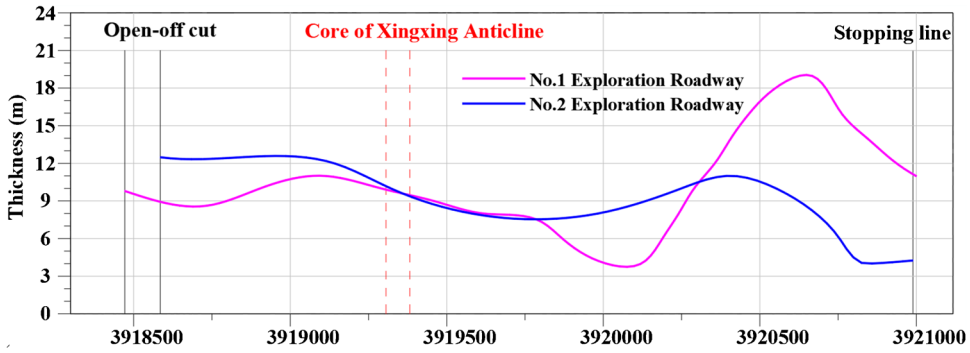

Fig. 3 Thickness of quaternary bottom aquifer

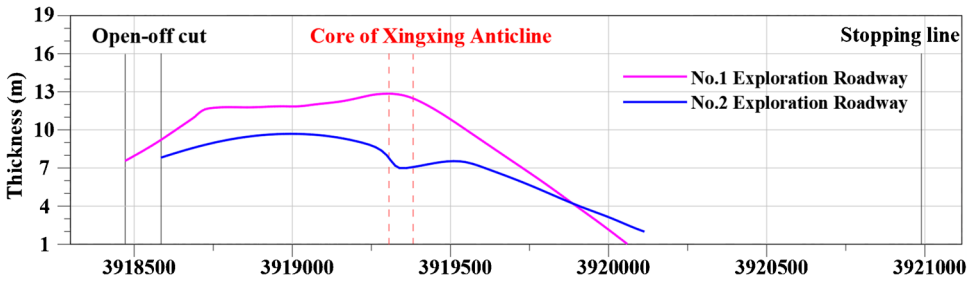

Fig. 4 Thickness of quaternary bottom aquifuge

Calculation of roof failure height

The mining of coal seam leads to the failure of roof overburden, forming caved zone, fractured zone, and sagging zone. The caved zone and fractured zone are collectively called the water-conducting fracture zone. The engineering geologic model of No. 3 coal seam roof is established (Fig. 6). The bedrock of the roof is divided into 11 layers, and we number them according to their distance from the coal seam. The physical and mechanical parameters of various rocks were obtained by testing the rock samples collected in the area studied.

Roof overburden failure model

Coal mining makes the roof overburden appear suspended distance, then the roof rock can be regarded as a simple beam fixed at both ends (Fig. 7).

When this overhanging distance exceeds the limit of the rock overhanging distance, the rock will fracture and collapse. The calculation equation of suspension distance is (Guo et al. 2019; Wang et al. 2021):

$$L_T = h_i\sqrt{\frac{2R_T}{(q_n)i + K_i}} \tag{1}$$

where L_T is the span of the roof, m; $(q_n)_i$ is the uniformly distributed load acting on the ith floor beam, kN/m; R_T is the ultimate tensile strength of the rock, MPa; h_i is the thickness of the rock layer ith, m; K_i is the self-weight load of the rock layer ith, kN/m.

$$(q_n)_i = \frac{E_i h_1^3(\gamma_i h_i + \gamma_{i+1}h_{i+1} + \cdots + \gamma_n h_n)}{E_i h_1^3 + E_{i+1}h_{i+1} + \cdots + \gamma_n h_n^3} \tag{2}$$

where $(q_n)_i$ is the uniformly distributed load acting on the ith floor beam, the load acting on the beam, kN/m; E_i is the elastic modulus of the rock layer ith, GPa; h_i is the thickness of the rock layer ith, kN/m; γ_i is the unit weight of the rock layer ith, kN/m^3.

Table 2 Lithologic assemblage of Jurassic and Permian bedrock

Borehole	Bedrock thickness (m)	Sandstone thickness (m)	Percentage of sandstone (%)	Mudstone thickness (m)	Percentage of mudstone (%)
O_2-13	110.0	71.9	65.3	38.1	34.7
2007–1	34.3	28.0	77.0	8.4	23.0
8–5	70.2	53.3	75.9	17.0	24.1
225	116.2	85.3	73.3	30.9	26.7
8–7	107.4	32.9	30.6	74.5	69.4

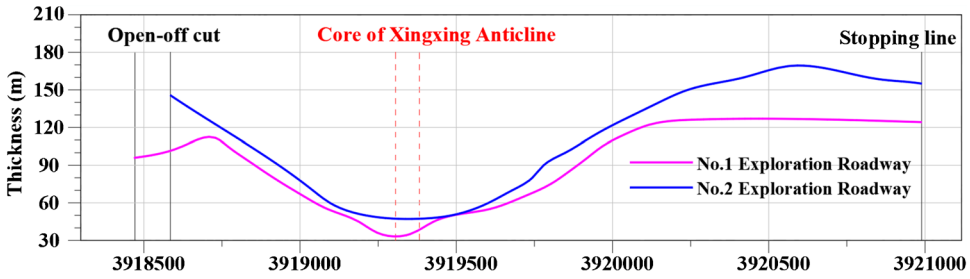

Fig. 5 Thickness of Jurassic and Permian bedrock

After caving occurs, one end of the rock layer is suspended and the other end is still fixed in the rock mass, which simplifies the rock layer into a cantilever beam (Fig. 8). The calculation equation of overhanging distance of rock stratum is:

$$L_s = h_i \sqrt{\frac{R_T}{3\left((q_n)_i + K_i\right)}} \tag{3}$$

where L_S is overhanging distance of rock stratum, m; h_i is the thickness of the rock layer ith, m; $(q_n)_i$ is the uniformly distributed load acting on the ith floor beam, the load acting on the beam, kN/m; K_i is the self-weight load of the rock layer ith, kN/m; R_T is the ultimate tensile strength of the rock, MPa.

As the coal seam continues to be mined, the overhanging distance of the rock strata increases. When the limit overhanging distance of the rock strata is exceeded, the rock strata will be broken and collapse again. This process occurs repeatedly in the mining of coal seam. Finally, due to the increase of bulging volume, the block produced by rock strata breaking will form voussoir beam (Qian and Liu 1984).

According to the voussoir beam theory, the goaf roof block basic mechanical structure is on the wall of mined-out area at the top of the block rotation and coal pillar at the top of the basic roof block extrusion and fracture between the formation of fault block in the horizontal direction, a horizontal force Ti mined-out area of basic roof rotation block above the half load borne by the mined-out area within the grind stone. The other half of the load is transferred from the compression between the broken blocks to the untapped pillars and faults ahead.

According to relevant studies (Guo et al. 2019; Wang et al. 2021), when the length of rock strata fault block meets Eq. (4), the whole masonry beam structure will lose stability, and we call the area that loses stability as caving zone, the area that is still stable is called fracture zone.

$$L_{ij} \le \frac{2(h_i - w_{ij})}{tg(\phi - \theta)} \tag{4}$$

where L_{ij} is the length of the block j of layer ith, m; w_{ij} is the vertical deformation of the block j (m); h_i is the thickness of the layer ith, m; φ is the friction angle at the contact,°.

When the suspension distance of the first layer does not exceed the ultimate suspension distance during coal seam mining, we believe that the rock layer is still in a stable state. The distance between the second layer and the first layer is:

$$\Delta_{i,i+1} = m - \sum_{i=1}^{i} h_i(K_p - 1) \tag{5}$$

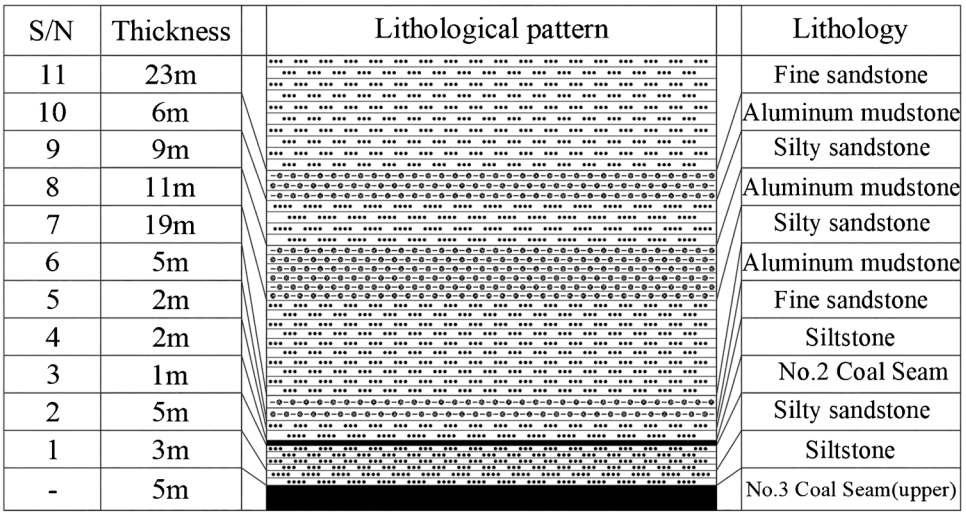

Fig. 6 Geological model of overburden

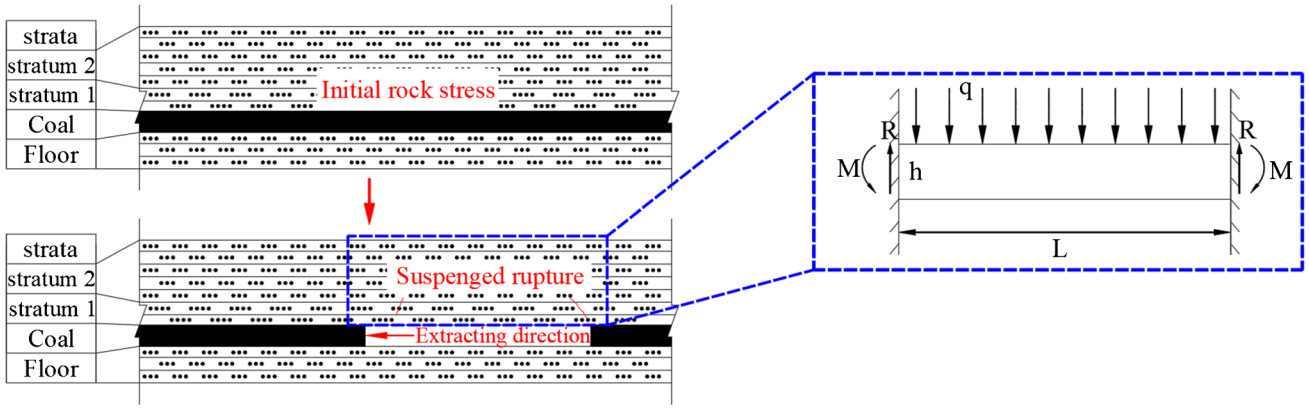

Fig. 7 Coal seam mining process and simply supported beam model

where $\Delta_{i,i+1}$ is the distance between layer *i*th and layer $i+1$th, m; m is the thickness of coal seam, m; h_i is the thickness of the layer *i*th, m; K_p is crushing expansion of rock.

When the distance between two adjacent rock layers is less than 0, the stability of the first rock layer does not affect the stability of the second rock layer, and the fracture zone will stop developing. The fracture zone will only extend to the first rock layer and the second rock layer will remain intact. (Table 3)

$$H = \sum_{i=1}^{i} h_i K_p \tag{6}$$

where H is the height of the fracture zone, m; h_i is the thickness of the layer *i*th, m; K_p is crushing expansion of rock.

By calculating the height of caved zone and fracture zone in the area studied with the above method in Eq. (6), overlying strata final abscission layer spacing and the height of fracture zone development of maximum height of 67.8 m are available; judging by Eq. (4), masonry beam structure stability and development of maximum caved zone height can be seen from Table 4, caving with maximum height to the roof on the 6th floor of coal seam, the maximum height of 19.4 m.

Empirical calculation of height of failure of overlying strata

In the long-term production practice of Yanzhou mining area, the empirical formula for Yanzhou mining area was summarized, which has been successfully applied to multiple coal faces in the mining area (Huang et al. 2007; Yu et al. 2019).

The empirical formula of caved zone height is:

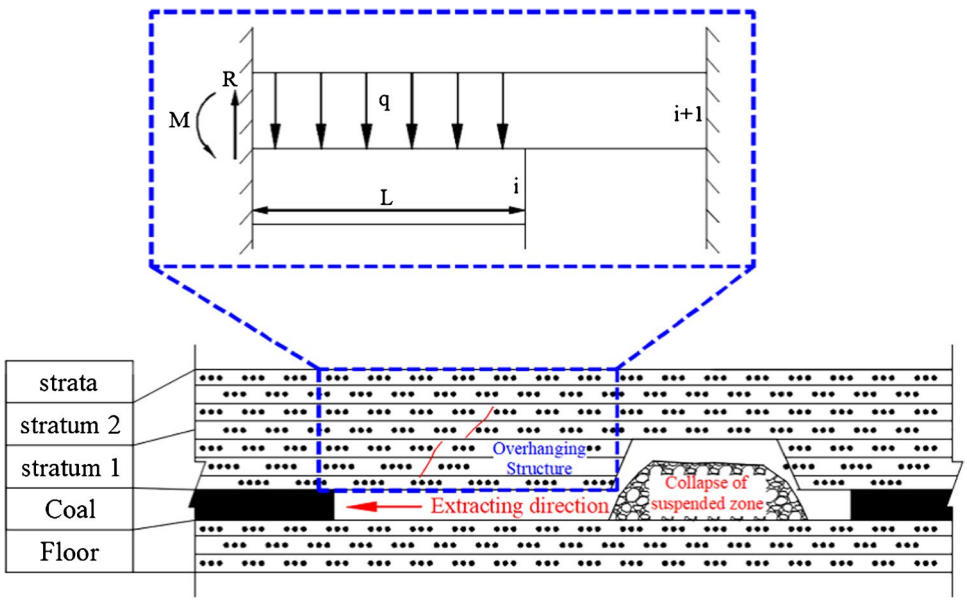

Fig. 8 Coal seam mining process and cantilever beam model

Table 3 Physical and mechanical parameters of bedrock layers

S/N	Lithology	h(m)	E(MPa)	R_T(MPa)	ρ(kg/m^3)	φ(°)
11	Fine sandstone	23	1100	2.5	2400	31
10	Aluminum mudstone	6	660	1.6	2100	27
9	Silty sandstone	9	1200	2.7	2500	30
8	Aluminum mudstone	11	660	1.6	2100	27
7	Silty sandstone	19	1200	2.7	2500	30
6	Aluminum mudstone	5	660	1.6	2100	27
5	Fine sandstone	2	1100	2.5	2400	31
4	Siltstone	2	860	2.4	2300	27
3	No. 2 coal seam	1	400	0.6	1400	22
2	Silty sandstone	3	1200	2.7	2500	30
1	Siltstone	5	860	2.4	2300	27

$$H_k = \frac{100\sum M}{2.13\sum M + 15.93} + 2.72 \tag{7}$$

$$H_k = \frac{100\sum M}{1.79\sum M + 19.97} + 3.20 \tag{8}$$

where H_k is the height of the caved zone, m; M is the thickness of the target coal seam by comprehensive mining, m.

The empirical formula of water-conducting fracture zone height is:

$$H_{li} = \frac{100M}{0.94M + 4.31} \pm 4.22 \tag{9}$$

For the area studied, the height of the caved zone and water-conducting fracture zone were calculated by these formulas. The mining thickness of the coal seam was calculated by using the average thickness of the target coal seam. The calculation results are shown in Table 5 (Figs. 9 and 10).

Table 4 Distance between each layer, height of each layer of overburden after fracturing and stability analysis of beam structure

S/N	Lithology	$\Delta_{i,i+1}$ (m)	h_iK_p (m)	L_{ij} (m)	$\frac{2(h_i-w_{ij})}{tg(\phi-\theta)}$(m)
11	Fine sandstone	—	—		
10	Aluminum mudstone	<0	3.18		
9	Silty sandstone	0.54	5.30		
8	Aluminum mudstone	1.34	1.20		
7	Silty sandstone	2.44	2.12	28.18	27.36
6	Aluminum mudstone	3.58	2.12	6.53	6.92
5	Fine sandstone	4.08	5.50	12.08	16.92
4	Siltstone	4.20	20.14	12.09	18.64
3	No .2 coal seam	4.32	12.10	5.22	16.43
2	Silty sandstone	4.52	9.54	16.44	19.66
1	Siltstone	4.82	6.60	14.80	17.14

Numerical simulation of overburden failure height

Geological model and modeling conditions

Based on the geological model in Fig. 6, a numerical model is developed with a size of 400×300×120 m (X×Y×Z). The average thickness of the No. 3 Coal Seam is 5 m. The model is extended to 86 m above the roof and 29 m below the floor. The overburden pressure due to gravity is calculated to be 4.25 MPa (Fig. 11). The following boundary conditions are imposed:

(1) The upper top boundary condition of the model is calculated based on the weight of the overlying strata ($\sum \gamma h$). For convenience, the distribution of the load is simplified to a uniformly distributed load, and the upper boundary condition is stress boundary conditions; that is, the gravity load of the overlying stratum that has a thickness of 170 m is about 4.25 MPa;
(2) The lower bottom boundary condition of the model is resting on hard rock, which has been simplified to be a displacement boundary condition. The model cannot move in the X and Y directions;
(3) The side boundary conditions: the boundary conditions on both sides of the model are solid rock mass, which is simplified as a displacement boundary condition, and the boundary can move along the Y direction while the fixed hinge supports movements in the X direction;

Table 5 Calculation results of empirical formula

Method		M /m	H_m /m	H_{li} /m
Empirical formulas	Formula (7)	5.0	21.5	
	Formula (8)	5.0	20.5	
	Formula (9)	5.0		59.71

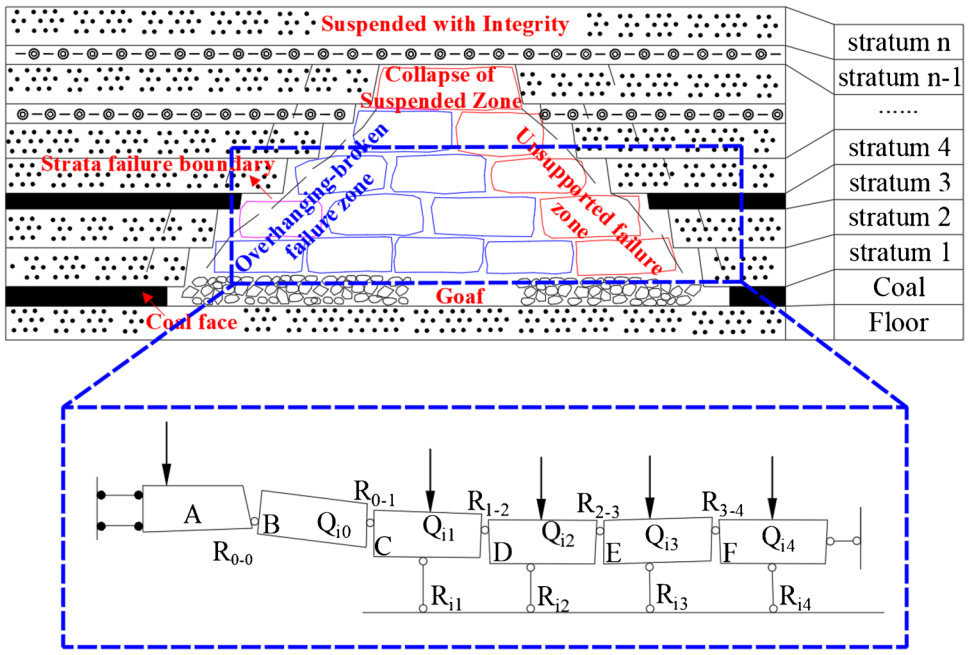

Fig. 9 Schematic diagram of masonry beam model structure

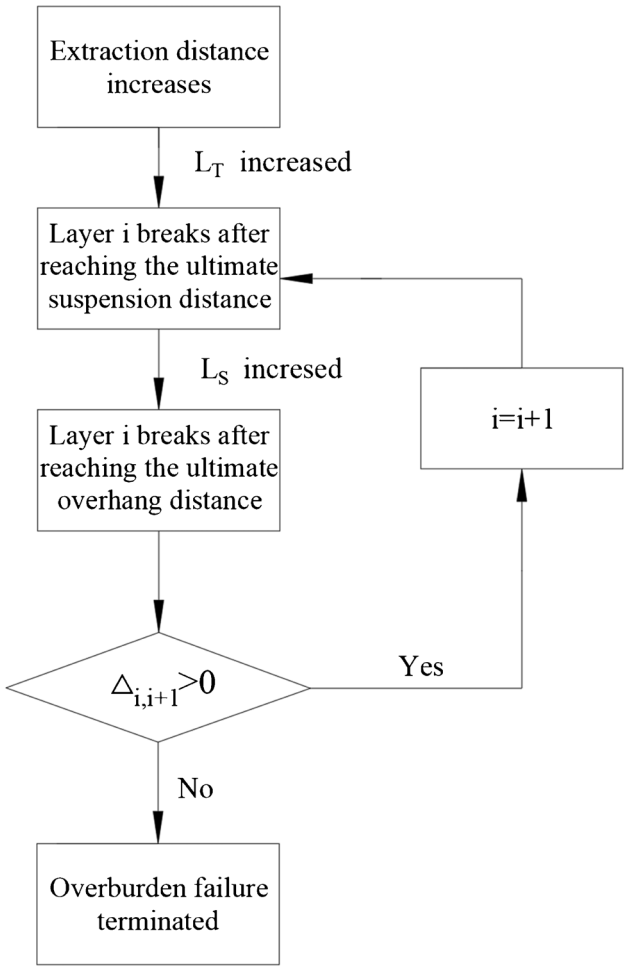

Fig. 10 Flowchart of roof overburden failure analysis (Wang et al. 2021)

Numerical simulation plan and results

A 3D model was constructed to determine the mined thickness of the working face; a more-coulomb model was the material constitutive model. In order to improve the calculation accuracy, arbitrary quadrilateral element was adopted, the surrounding element was encrypted, and the model was discretized with a total of 64,800 elements and 69,905 nodes (Fig. 12).

The calculation parameters of Table 3 were used for the numerical simulation which was carried out by using FLAC^{3D}. The range of the work face to be mined is $200 \times 100 \times 5$ m. In the working face propulsion scheme, the coal seam shall start from the position of 100 m in the X direction and leave 100 m coal pillars at both ends of the X direction, mining 120 m in the Y direction, with 90 m coal pillars at both ends. The model adopts a step-by-step excavation method, with each excavation distance of 20 m and excavation for 10 times.

The change rules of the plastic zone when the working face is advanced by 20 m, 40 m, 60 m, 80 m, 100 m, 120 m, 140 m, 160 m, 180 m, and 200 m are mainly analyzed to study the development and evolution rules of each failure zone. The numerical simulation results of the distribution rules of the plastic zone are shown in Fig. 13.

Analysis of overburden failure height

According to the deformation and failure of the plastic zone, Origin is used to carry out fitting analysis on the height value of the caved zone and the height value of the

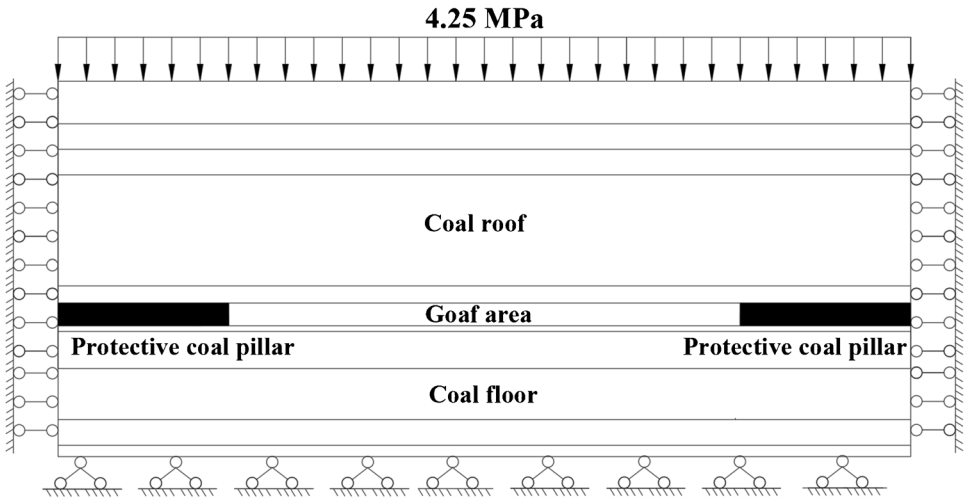

Fig. 11 Surface stratigraphy of initial and boundary conditions

water-conducting fracture zone, and the correlation relationship is shown in Fig. 14.

In combination with the simulation results obtained in Figs. 13 and 14, the development heights of caved zone and water-conducting fracture zone are analyzed. In the process of work face mining, the natural stress of overlying strata is changed, and a plastic zone is formed in the numerical simulation software. The height of caved zone and water-conducting fracture zone is distinguished by the strength criterion and rock mechanics parameters, which the middle and both sides are the same as the height of the caved zone and water-conducting fracture zone development respectively.

The dynamic development of caved zone and water-conducting fracture zone in overlying rock is shown in Fig. 13. When the work face is extracted by 20 m, the plastic variation range of overburden rock is lesser, and the goaf is directly caved and filled. The height of caved zone is 2.5 m, and the height of water-conducting fracture zone is 7.5 m. When the work face is extracted by 40 m, when the overlying strata collapse, the plastic failure zone of overlying rocks continues to develop upward and the development height increases. The height of caved zone is 5.1 m, and the height of water-conducting fracture zone is 15.9 m. When the work face is extracted by 60 m, the overlying rock failure continues to develop upward, and the fractured fine sand rock forms voussior beam, presenting a relatively obvious saddle-shaped failure. The height of caved zone is 7.5 m, and the height of water-conducting fracture zone is 25.0 m. When the work face is extracted by 80 m, several rocks strata break, the plastic failure of overlying rock develops rapidly in the longitudinal direction, and the scope of saddle-shaped failure is further enlarged. The height of caved zone is 14.5 m, and the height of water-conducting fracture zone is 45.2 m. When the work face is extracted by 100 m, the plastic failure zone of overlying rock continues to develop rapidly upward to reach full subsidence. The height of caved zone is 20.1 m, and the height of water-conducting fracture zone is 63.3 m. When the work face continued to extract

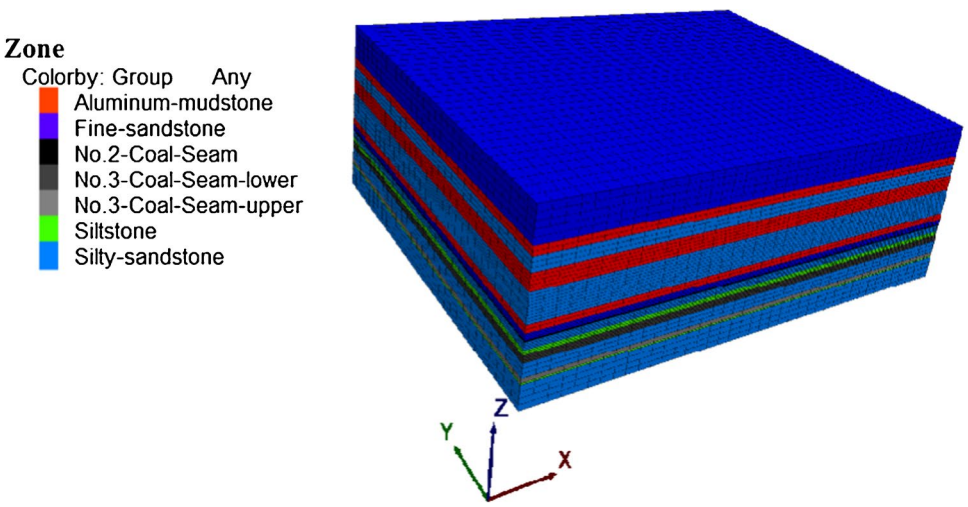

Fig. 12 Numerical model of mine

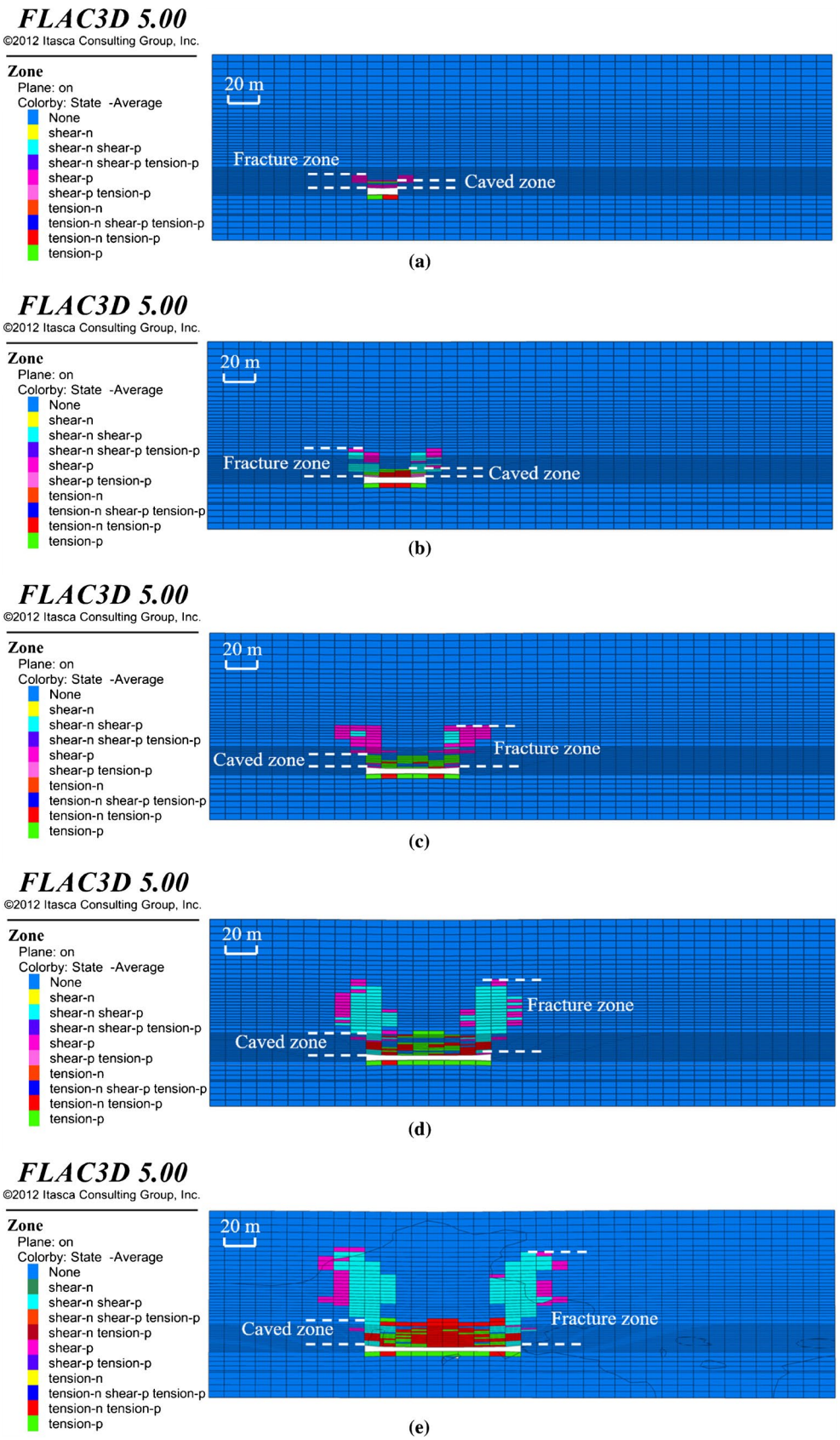

Fig. 13 Distribution diagram of mining plastic area of overburden in No.3 coal seam

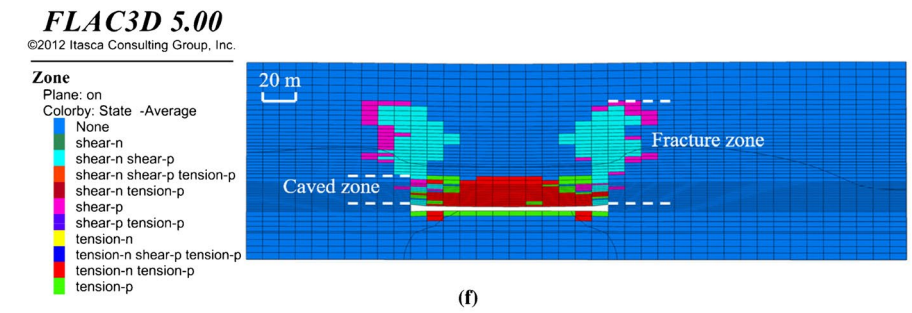

(f)

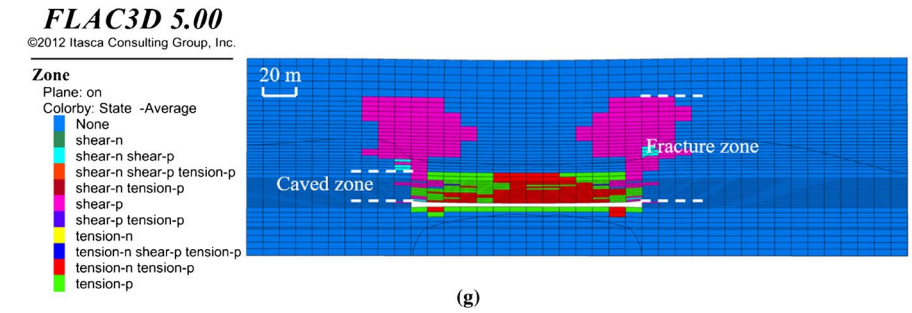

(g)

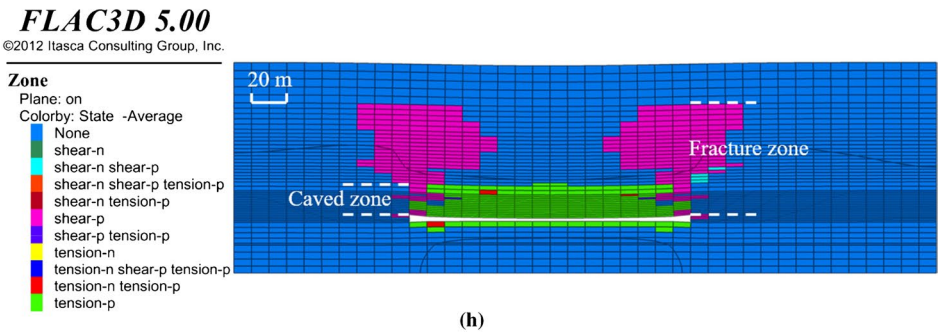

(h)

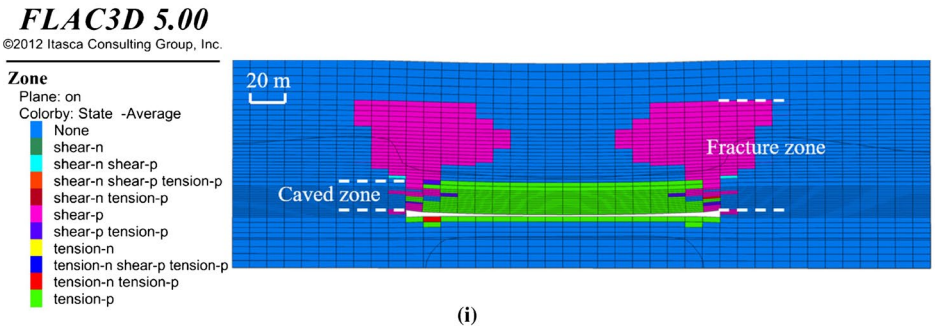

(i)

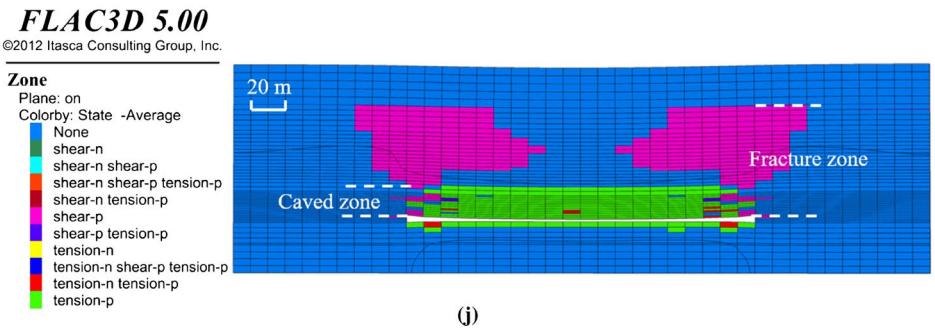

(j)

Fig. 13 (continued)

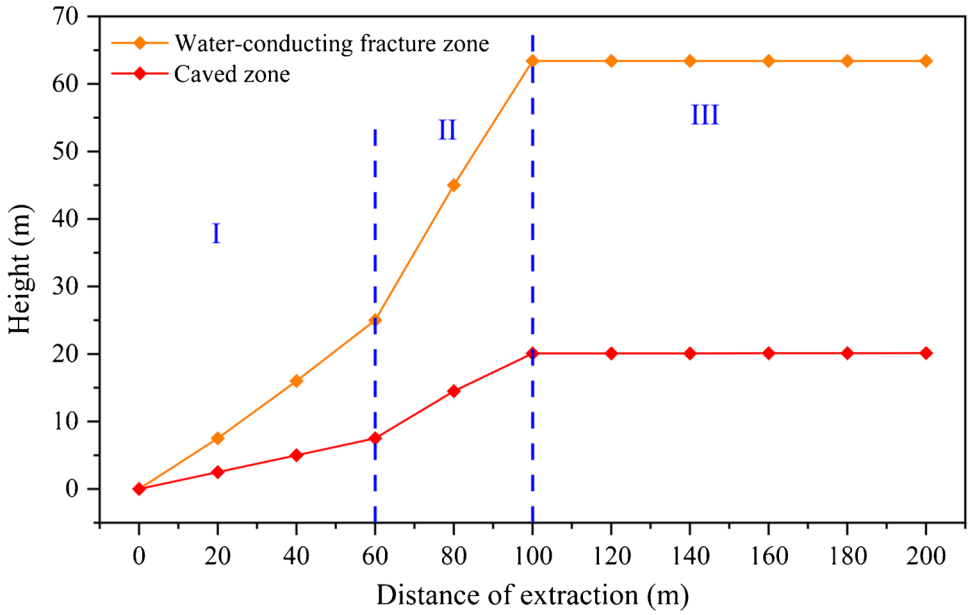

Fig. 14 The height fitting of caved zone and water-conducting fracture zone

up to 200 m, the plastic failure of overlying rock mainly develops in the transverse direction and basically stops in the longitudinal direction after full subsidence. The height of caved zone and water-conducting fracture zone remains basically unchanged.

Through numerical simulation, it is found that in the process of overlying rock failure developing upward, the caved zone is formed by directly roof filling the goaf in the form of caving. Due to the supporting function of the caved rock block, the overlying rock layer will hinge to form a beam structure, and the fracture block degree of the overlying rock layer will be reduced to form a fracture zone. The water-conducting fracture zone is transmitted upward in the form of voussior beam and separations, and the rock strata below the separations are bent and deformed until the limit variable is reached, which is connected with longitudinal fractures and finally forms the apex of the fracture zone. The height change curve of caved zone and water-conducting fracture zone in the process of working face propulsion is represented in Fig. 14; the change of overburden failure height can be divided into three stages:

Slow increase stage (I): between the open cut of work face and extraction of 60 m, the direct top reaches the ultimate span, the unstable caving and filling goaf is reached, the plastic change range of overburden is small, and the development speed is slow, the failure rate of overburden is slow, and the height of caved zone and water-conducting fracture zone increases linearly.

Rapid growth stage (II): The work face is extracted from 60 to 100 m, due to the change in the stress state of the overlying rock due to mining, stress concentration occurs on both sides of the working face, and the rock strata are often subjected to shear failure and some rock formations are broken. The plastic failure of overlying rock develops rapidly in the longitudinal direction and the height of caved zone and water-conducting fracture zone increases rapidly.

Stabilization stage (III): The work face is extracted from 100 to 200 m, due to the crushing and swelling property and bearing capacity of caved rock blocks in the goaf, voussoir beam structure is formed after the overlying rock breaks, and the caved rock further fills and compacts the goaf in a temporary stable state. The cantilever beam and voussior beam structure of the caved zone are transmitted periodically

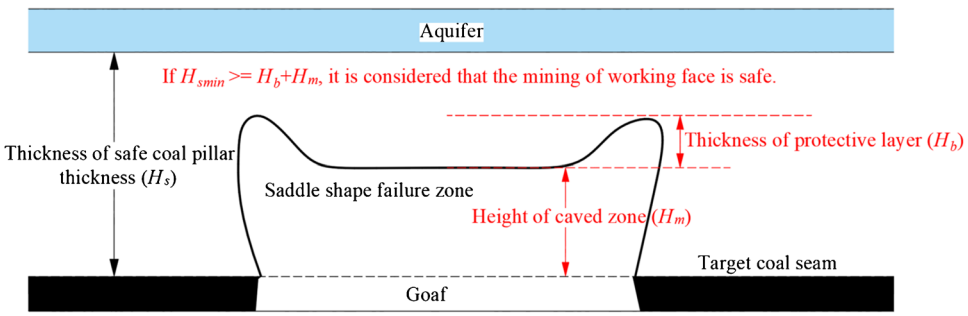

Fig. 15 Principle of retaining safe coal pillar

Table 6 Recommended value of protective layer thickness

Location of the working surface	Mining thickness M (m)	Protective layer thickness H_b (m)	H_b/M	Reference
Xinglongzhuang Coal Mine Working Face 2304	7.1	11.5	1.6	Huang et al. 2007
Xinglongzhuang Coal Mine Working Face 23S1	5.7	9.4	1.65	Huang et al. 2007
Baodian Coal Mine Working Face 83–01	5.8	8.7	1.5	Yu et al. 2019
Baodian Coal Mine Working Face 83–02	5.0	7.5	1.5	Area studied

to the propulsion direction respectively, and the overburden failure height reaches the maximum and remains stable. The height of caved zone and water-conducting fracture zone basically remains unchanged and no longer develops upward. At this time, the plastic failure area mainly develops in the transverse direction, and the transverse failure area increases.

Since shear failure usually takes place in the plastic zone, the plastic zone can be used to determine the failure height of the roof based on the saddle-shaped damage to the roof after mining takes place. The heights of the caved and the water-conducting fracture zones can be determined based on the amount of deformation. The calculated height of the caved zone is about 20.0 m while that of the water-conducting fracture zone is about 63.3 m.

Determination of height of waterproof coal pillar

The safety requirement of mining under water for the height of roof bedrock is that the minimum bedrock thickness is greater than the sum of the height of caved zone and the thickness of protective layer (Fig. 15). It is considered that such bedrock conditions can meet the needs of safe mining.

$$H_{s(min)} \geq H_m + H_b \tag{10}$$

where $H_{s(min)}$ is the minimum recommended value of safe coal pillar, m; H_m is the maximum height of the caved zone, m; H_b is the thickness of protective layer, m.

For the selection of protective layer thickness, the successful experience of several coal mining faces in Yanzhou mining area is adopted (Huang et al. 2007; Yu et al. 2019). The Xinglongzhuang coal mine and Baodian coal mine are adjacent to each other and belong to Yanzhou mining area, and working face 83–01 is is only tens of meters adjacent to the area studied (Table 6). The stratigraphic conditions of these working faces are basically the same. We think the successful experience of these working faces is of great reference value and can be applied to the area studied by analogy. The recommended value of protective layer thickness (H_b) in the area studied is 1.5 times of mining thickness (M), $H_b = 1.5\ M$. The average mining thickness of coal seam is taken for calculation, $H_b = 1.5 \times 5 = 7.5$ m. Combined with the above height calculation of caved zone and water-conducting fracture zone height, the recommended value of safe coal pillar can be obtained.

In order to ensure the safety of mining as much as possible, the maximum value (29.0 m) in the result is selected as the recommended value of the minimum value of safe coal pillar (H_{smin}) (Table 7). The minimum value of coal seam roof bedrock in the area studied is 34.3 m, which is greater than the minimum recommended value of safe coal pillar. It is considered that it is safe to carry out coal seam mining when the bedrock thickness on the roof of the target coal seam is greater than the recommended value of safe coal pillar.

Table 7 Recommended value of safe coal pillar

Method		H_{li} (m)	H_m (m)	H_b (m)	$H_{s(min)}$
Theoretical calculation		67.8	19.4	7.5	26.9
Empirical formulas	Formula (7)	–	21.5	7.5	29.0
	Formula (8)	–	20.5	7.5	28
	Formula (9)	59.71	–	–	–
Numerical simulation		63.3	20.0	7.5	27.5

Conclusions

Through theoretical analysis, empirical formula, and numerical simulation, the height of caved zone and water-conducting fracture zone height in the area studied are calculated, the thickness of protective layer is determined by analogy, and finally the minimum recommended value of safe coal pillar is put forward. The specific conclusions are as follows:

(1) From the perspective of safe mining, the height of the caved zone and water-conducting fracture zone obtained by the three methods are compared. Finally, the height of the caved zone is 21.5 m and the height of the water-conducting fracture zone is 67.8 m.
(2) Combined with the drilling data in the study area, the minimum value of coal seam roof bedrock in the study area is 34.3 m, which is greater than the minimum rec-

ommended value of safe coal pillar (29.0 m). It is considered that the roof bedrock of the target coal seam meets the requirements of safe coal pillar retention and can be safely mined.

Acknowledgements The authors are grateful to the anonymous reviewers for their helpful comments on the manuscript.

Funding This research is supported by the Postgraduate Research and Practice Innovation Program of Jiangsu Province (KYCX21_2315), Assistance Program for Future Outstanding Talents of China University of Mining and Technology (2021WLJCRCZL005) and the Priority Academic Program Development of Jiangsu Higher Education Institutions (PAPD).

Declarations

Conflict of interest The authors declare that they have no competing interests.

References

Cao SG, Miao XX, Qian MG (1998) Stability and application of bond-beam structure. Coal Technol Northeast China 5:22–26 (in chinese)

Ghasemi E, Shahriar K (2012) A new coal pillars design method in order to enhance safety of the retreat mining in room and pillar mines. Safety Sci 50(3):597–585

Guo WB, Zhao GB, Lou GZ, Wang SR (2019) A new method of predicting the height of the fractured water-conducting zone due to high-intensity longwall coal mining in China. Rock Mech Rock Eng 52(8):2789–2802

Huang Z, Zeng W, Wu Y, Li SJ, Gu QX, Zhao K (2021) Effects of temperature and acid solution on the physical and tensile mechanical properties of red sandstones. Environ Sci Pollut Res 28:20608–20623

Ju MH, Li XH, Yao QL, Liu SY, Liang S (2017) Effect of sand grain size on simulated mining-induced overburden failure in physical model tests. Eng Geol 226:93–106

Li N, Wang EY, Ge MC (2015) The fracture mechanism and acoustic emission analysis of hard roof: a physical modeling study. Arab J Geosci 8(4):1895–1902

Liu SL, Li WP, Wang QQ (2018) Height of the water-flowing fractured zone of the jurassic coal seam in Northwestern China. Mine Water Environ 37(2):312–321

Qian MG, Liu TC (1984) Mine pressure and control. China Coal Industry Publishing House, Beijing

Qian MG, Miao XX, He FL (1994) Analysis of key block in the structure of voussoir beam in longwall mining. J China Coal Soc 6:557–563 (in chinese)

Sui WH, Hang Y, Ma LX, Wu ZY, Zhou YJ, Long GQ, Wei LB (2015) Interactions of overburden failure zones due to multiple-seam mining using longwall caving. B Eng Geol Environ 74(3):1019–1035

Sun W, Zhang Q, Luan YH, Zhang XP (2018) A study of surface subsidence and coal pillar safety for strip mining in a deep mine. Environ Earth Sci 77(17):627–643

Wang Q, Gao HK, Jiang B, Li SC, He MC, Wang DC, Lu W, Qin Q, Gao S, Yu HC (2017) Research on reasonable coal pillar width of roadway driven along goaf in deep mine. Arab J Geosci 21(10):466–482

Wang F, Xu JL, Xie JL (2019) Effects of arch structure in unconsolidated layers on fracture and failure of overlying strata. Int J Rock Mech Min 114:141–152

Wang XH, Zhu SY, Yu HT, Liu YX (2021) Comprehensive analysis control effect of faults on the height of fractured water-conducting zone in longwall mining. Nat Hazards 108(2):2143–2165

Wu GM, Bai HB, Du B, Wu LY, He SX, Li H (2019) Study on the failure mechanism of clay layer overlying thin bedrock in coal seam mining. Environ Earth Sci 78:315–337

Wu Y, Huang Z, Zhao K, Zeng W, Gu QX, Zhang R (2020) Unsteady seepage solutions for hydraulic fracturing around vertical wellbores in hydrocarbon reservoirs. Int J Hydrogen Energ 14:2263

Wu Y, Li XZ, Huang Z, Xue S (2021) Effect of temperature on physical and mechanical and acoustic emission properties of Beishan granite, Gansu Province. China Nat Hazards 107(2):1577–1592

Xu WT, Li XZ, Zhang YS, Wang XY, Liu RC, He ZC, Fan J (2021) Aperture measurements and seepage properties of typical single natural fractures. Bull Eng Geol Environ 80:8043–8058

Yang WF, Xia XH, Zhao GR, Ji YB, Shen DY (2011) Overburden failure and the prevention of water and sand inrush during coal mining under thin bedrock. Min Sci Technol 21(5):733–736 (in chinese)

Ye Q, Wang G, Jia ZZ, Zheng CS, Wang WJ (2018) Similarity simulation of mining-crack-evolution characteristics of overburden strata in deep coal mining with large dip. J Petrol Sci Eng 165:477–487

Yu ZB, Zhu SY, Guan YZ, Hu DX (2019) Feasibility of modifying coal pillars to prevent sand flow under a thick loose layer of sediment and thin bedrock. Mine Water Environ 38(4):817–826

Zhao KY, Xu NX, Mei G, Tian H (2016) Predicting the distribution of ground fissures and water-conducted fissures induced by coal mining: a case study. Springerplus 5:977–1002

Zhao YH, Wang SR, Zou YF, Wang XC, Huang BQ, Zhang XG (2018) Pressure-arching characteristics of fractured strata structure during shallow horizontal coal mining. Teh Vjesn 25(5):1457–1466

Zhou DW, Wu K, Bai ZH, Hu ZQ, Li L, Xu YK, Diao XP (2019) Formation and development mechanism of ground crack caused by coal mining: effects of overlying key strata. B Eng Geol Environ 78(2):1025–1044

Zhu SY, Jiang ZQ, Zhou KJ, Peng GQ, Yang CW (2014) The characteristics of deformation and failure of coal seam floor due to mining in Xinmi coal field in China. B Eng Geol Environ 73(4):1151–1163